Radiology

Ten Things You Might Not Know about Iron Oxide Nanoparticles[1]

Heike E. Daldrup-Link, MD, PhD

Amid mounting concerns about nephrogenic sclerosis and gadolinium deposition in the brain, physicians and patients alike are starting to question the use of gadolinium chelates for clinical magnetic resonance (MR) imaging. The search for safer alternatives is currently underway. In North America, the iron supplement ferumoxytol has gained considerable interest as an MR contrast agent. In Europe, ferumoxtran-10 is entering phase III clinical trials. As these agents are starting to be used by a new generation of radiologists, important clinical questions have reemerged, including those that have been answered in the past. This article offers 10 important insights for the use of iron oxide nanoparticles in clinical MR imaging.

Online SA-CME
See www.rsna.org/education/search/ry

Learning Objectives:

After reading the article and taking the test, the reader will be able to:

- Describe important safety aspects of superparamagentic iron oxide nanoparticles
- Describe the diagnostic value of iron oxide nanoparticles for MR imaging applications
- Explain which technical parameters can optimize the sensitivity and specificity of ferumoxytol-enhanced MR images
- Describe intrinsic immune-modulating therapeutic effects of iron oxide nanoparticles

Accreditation and Designation Statement

The RSNA is accredited by the Accreditation Council for Continuing Medical Education (ACCME) to provide continuing medical education for physicians. The RSNA designates this journal-based SA-CME activity for a maximum of 1.0 *AMA PRA Category 1 Credit*™. Physicians should claim only the credit commensurate with the extent of their participation in the activity.

Disclosure Statement

The ACCME requires that the RSNA, as an accredited provider of CME, obtain signed disclosure statements from the authors, editors, and reviewers for this activity. For this journal-based CME activity, author disclosures are listed at the end of this article.

[1] From the Department of Radiology, Molecular Imaging Program at Stanford (MIPS), Department of Pediatrics, and Institute for Stem Cell Biology and Regenerative Medicine, Lucile Packard Children's Hospital, Stanford University, 725 Welch Rd, Room 1665, Stanford, CA 94305-5614. Received December 3, 2016; revision requested January 4, 2017; final revision received January 14; accepted February 1; final version accepted February 23. **Address correspondence to** the author (e-mail: *H.E.Daldrup-Link@stanford.edu*).

Supported by Eunice Kennedy Shriver National Institute of Child Health and Human Development (5HD081123), the National Cancer Institute (R21CA190196, R21CA176519), and the National Institute of Arthritis and Musculoskeletal and Skin Diseases (4R01AR054458-09, R21AR066302).

In the late 1970s, Lauterbur and colleagues discovered that paramagnetic ions could influence proton relaxation times on magnetic resonance (MR) images (1). The first volunteer was injected with gadopentetate dimeglumine in 1983 (2,3). Although early clinical studies primarily focused on gadolinium chelates, MR investigators had already identified iron compounds such as ferric ion (Fe^{3+}) as alternate MR contrast agents with high r1 relaxivities (4). During the next decades, superparamagnetic iron oxide (SPIO) nanoparticles were developed for limited and well-defined clinical applications such as MR angiography, tissue perfusion studies, and atherosclerotic plaque and tumor imaging. Amid recent concerns about nephrogenic sclerosis and gadolinium deposition in the brain, patients and physicians are questioning the use of gadolinium chelates and are actively seeking alternatives. In North America, the iron supplement ferumoxytol has gained considerable interest as an MR contrast agent. Ferumoxytol is composed of SPIO nanoparticles with strong T1 and T2 relaxivities and therefore can be used "off label" to enhance soft-tissue contrast on MR images. In fact, ferumoxytol was originally designed as an MR contrast agent, but was later developed for anemia treatment (5,6). In North America, ferumoxytol (Feraheme) is increasingly being used for MR imaging (5,7–11). In parallel, the iron oxide nanoparticle compound ferumoxtran-10 (Sinerem/Combidex) has gained a surge of interest in Europe and is currently under clinical development (12–15). As these agents are adopted by a new generation of radiologists, it is important to build on the many lessons learned from previous experience with iron oxide nanoparticle compounds. As a researcher who has worked with iron oxide nanoparticles for more than 20 years, I have noticed the re-emergence of important clinical questions that have already been answered. This article addresses these newly resurfaced questions and offers 10 key insights into the use of iron oxide nanoparticles for clinical MR imaging.

Essentials

- Ultrasmall superparamagnetic iron oxides can cause immune responses through the classic Gell-Coombs pathway or complement activation-related pseudoallergy.
- Extravasation of iron oxide nanoparticles can cause long-lasting skin discolorations.
- Dual–contrast agent MR imaging studies can be obtained after injecting iron oxides and then gadolinium chelates or vice versa.
- Iron can be retained in the choroid plexus.
- Ferumoxytol enhancement of lymph nodes is not due to macrophage phagocytosis.

Imaging Applications for Ferumoxytol and Ferumoxtran-10 Build on Decades of Experience with Iron Oxide Nanoparticles

SPIO nanoparticles have been used for clinical imaging for more than 20 years (16–21). Because of their size (mean hydrodynamic diameter > 50 nm), almost all SPIOs are rapidly phagocytosed by Kupffer cells in the liver (16–19). As such, SPIOs have been widely used for liver imaging in patients in North America and Europe. However, many SPIOs were recently taken off the market due to their limited spectrum of applications; Resovist is the only SPIO still being distributed for clinical liver imaging in Japan. The majority of companies have prioritized the development and distribution of ultrasmall SPIOs (USPIOs, mean hydrodynamic diameter < 50 nm) (7,12,22,23). USPIOs have a longer blood half-life than SPIOs and therefore can be used for a wider spectrum of imaging applications, such as MR angiography (7,9,24,25), tumor perfusion imaging (9,23,26), liver imaging (14), lymph node imaging (11,12,15,22), bone marrow imaging (27), atherosclerotic plaque imaging (28–30), and imaging of various types of inflammation (31–33). Food and Drug Administration (FDA) approval of the iron supplement ferumoxytol (Feraheme) has led to a renaissance of "off-label" use USPIO for a variety of imaging applications (7–11,32,34). Instead of reinventing the wheel, we can build on existing experience with other USPIOs, such as ferumoxtran-10 (12,13,30,32), ferucarbotran/SHU555C (32), and feruglose (23,35), to truly advance the field of nanoparticle imaging. Before USPIOs entered clinical trials, these nanoparticles were labeled and described by identifying numbers. When reviewing literature about a specific iron oxide product, these initial formulations should be included to capture all available information. An overview of the synonyms for different intravenously administered iron oxide nanoparticles is provided in the Table. Please note that Medline lists more than 7000 articles on clinical iron oxide nanoparticles. The literature cited here support selected clinical questions, but is not meant to be comprehensive.

Strategies to Prevent and Minimize Adverse Reactions to USPIOs

Several investigators have described serious and life-threatening anaphylactic reactions to intravenously administered ferumoxytol nanoparticles (36,37). The aggregate rate of serious adverse events was 0%–1%, and the aggregate rate of anaphylaxis was 0.02%–0.2% (5,38,39). In response, the FDA has issued a black box warning

https://doi.org/10.1148/radiol.2017162759

Content codes: MR MI

Radiology 2017; 284:616–629

Abbreviations:
FDA = Food and Drug Administration
IP = in phase
OP = opposed phase
RES = reticuloendothelial system
SPIO = superparamagnetic iron oxide
USPIO = ultrasmall SPIO

Conflicts of interest are listed at the end of this article.

Characteristics of Widely Used Clinical Iron Oxide Nanoparticles

Generic Name and Product No.	Trade Name	Coating	Hydrodynamic Diameter	Blood Half-Life in Patients	References
Ferumoxides AMI-24	Endorem Feridex	Dextran	SPIO: 50–100	10 minutes	16,17,19,77,80
Ferucarbotran SHU555A	Resovist* (Japan)	Carboxy-dextran	SPIO: 60–80 nm	12 minutes	18,20,21,76
Ferumoxtran-10 AMI-227	Sinerem* (Europe)	Dextran	USPIO: 20–50 nm	> 24 hours	12,22
Ferucarbotran SHU555C	Resovist S Supravist	Carboxy-dextran	USPIO: 20–25 nm	6–8 hours	33
Feruglose NC100150	Clariscan	Carbohydrate-polyethylene glycol	USPIO: 11–15 nm	2 hours	23
Ferumoxytol AMI-7228	Feraheme* (North America)	Carboxy-methyldextran	USPIO: 20–30 nm	10–14 hours	10,34,37,113

Note.—The most widely used clinical products are listed, which have been used in hundreds of patients and in multiple countries. The letters in front of the product numbers indicate the company that developed the agent: AMI = Advanced Magnetic Imaging, SHU = Schering, NC = Nycomed. Since the final clinical product may be licensed to other companies, the company that commercially distributes the agent to radiology practices can be different in different countries and different years.

* Agents that are currently (as of 2017) available for use in patients in the aforementioned countries

regarding these risks (40). The FDA recommends that clinicians carefully consider the potential risks and benefits of administering ferumoxytol, especially in elderly patients who have a higher risk of adverse events and patients with a history of allergic reactions to any iron product. In addition, the FDA urges clinicians to only infuse ferumoxytol intravenously when diluted in 50–200 mL of 0.9% sodium chloride or 5% dextrose solution and administer it slowly over a minimum of 15 minutes. Patients should then be closely monitored for signs and symptoms of allergic reactions for at least 30 minutes (40).

USPIOs can cause immune responses according to the Gell-Coombs system (Fig 1) (41). The classic pathway involves a type III dextran reactive antibody reaction with the formation of immune complexes and complement activation. A number of preventive strategies have been applied to reduce the incidence of these reactions. Some investigators have prescribed aspirin prior to USPIO administration (42) based on previous reports that aspirin can inhibit complement activation and prevent hemodynamic reactions to liposomes in animal models (43). In addition, low-molecular-weight dextrans administered prior to USPIO have been reported to block circulating antidextran antibodies (or antibodies that cross-react with dextran) (44). For instance, isomaltoside 1000 has been suggested to act as a monovalent antigen (ie, hapten) by blocking the antibody binding sites without the formation of immune complexes (45).

Figure 1

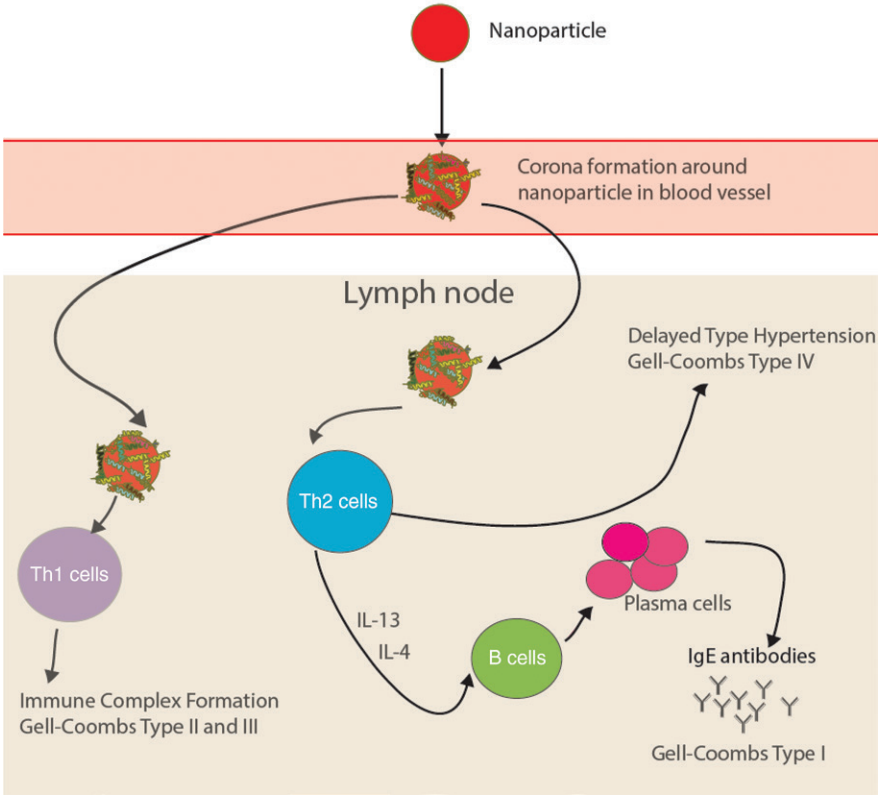

Figure 1: Overview of possible immune response mechanisms against ferumoxytol nanoparticles according to the Gell-Coombs system.

Rapid injection of iron products can cause a distinct nonimmune reaction: complement activation-related pseudoallergy (CARPA) (46–49). Ferumoxytol contains a small amount of free iron (< 0.002% of the total iron content), independent of the liquid used for dilution (45). This free iron can activate the complement system, lead to mast

cell degranulation, and cause anaphylactic-like symptoms with severe hypotension and/or severe flush sensations (50). This reaction can be alleviated by slow infusion of diluted iron products. Other investigators have suggested that injecting iron too rapidly can exacerbate CARPA by exceeding the clearance rate of anaphylatoxins from the blood by carboxypeptidase N and macrophages (47,48). Regardless of the underlying cause, hypotensive reactions observed with rapid ferumoxytol injections led the FDA recommendation to administer diluted ferumoxytol slowly under continuous blood pressure monitoring. Patients with cardiac preconditions are particularly vulnerable to iron-induced hypotensive reactions because they do not have the cardiac reserve to compensate for a hypotensive crisis. Iron-induced hypotension is best treated with intravenous fluid. Antihistamines can escalate hypotensive events and reactive tachycardia (51). Since clinical presentations of CARPA and true anaphylaxis can overlap; guidelines for the treatment of iron-induced adverse events recommend fluid administration in conjunction with other drug therapies for anaphylactic reactions (46).

Filters Are No Longer Used

In the absence of an external magnetic field, USPIOs have little tendency for self-aggregation and are stabilized as individual particles by their synthetic coat (52). However, micro-oxidation, microrelease of ferrous ions, and electrostatic interactions can promote natural aggregation. In addition, compared with first-generation SPIOs, USPIOs have a higher relative surface area and number of surface atoms, which can promote agglomeration. Due to this concern, for nearly 20 years both SPIOs and USPIOs had to be administered through a 5-μm (18–23) or 0.22-μm filter (27). This filter was placed between the syringe and infusion line and/or the intravenous access to the patient, with the goal of preventing injection of nanoparticle aggregates. However, there is a lack of scientific evidence showing that using a filter actually reduces nanoparticle aggregates in a solution injected into a patient. Thus, filters are no longer used for administration of these nanoparticles.

Increasing temperature has been shown to decrease the enthalpy of nanoparticles (53); for instance, when nanoparticles are dissolved in cool saline, a negative enthalpy change can occur, for which the system may compensate by maximizing the existing entropy and separating liquid molecules from nanoparticles, thereby promoting aggregation. Many current USPIO formulations contain citrate, which binds ferric ions and prevents nanoparticle aggregation (45). Systematic studies are needed to evaluate the effect (or lack thereof) of varying compositions and temperatures of clinical USPIO solutions on nanoparticle agglomeration.

Iron Oxide Nanoparticles Can Cause Local Side Effects at the Infusion Site

Patients should be informed that extravasation of iron oxide nanoparticles can cause long-lasting skin discolorations (brown areas) of the skin surrounding the infusion site. Such discolorations will persist for several months but usually slowly disappear over time, similar to an organic tattoo. A clinical intervention to accelerate the disappearance of this discoloration would be valuable. In fact, iron-induced skin discoloration is one reason a skin prick test for an allergic reaction is considered neither feasible nor safe. The by-products of the pigments' decomposition accumulate in the lymphatic system and can cause detectable signal changes of local lymph nodes on MR images.

Usually, iron oxide nanoparticles are inert and do not cause local inflammatory reactions. However, rarely, extravasated iron products can cause granulomas, dermatitis, or local fibrosis. In animal experiments, locally administered iron dextran products inhibited the growth of subcutaneous tumors through a Fenton reaction and production of reactive oxygen species (54). Additionally, intramuscularly injected iron products have been associated with the development of sarcomas (55). The number of patients who received intramuscular injections of iron compounds is unknown but is probably very small; thus, available data to date do not support a strong risk of tumor development in patients (56). However, increased iron concentrations in leg ulcers of patients caused significantly impaired wound healing (57), and increased iron concentrations in rats with peritonitis exacerbated inflammation-mediated peritoneal damage (58). These findings were noted at iron tissue concentrations much above the concentrations reached after intravenous USPIO doses for imaging purposes and can be explained by iron oxide-induced chronic inflammation and reactive oxygen species production. Further studies are needed to evaluate potential intrinsic immune-modulating effects of iron oxide nanoparticles in patients.

Protein Coronas Form around Iron Oxide Nanoparticles in Serum

Proteins in blood and serum form a protein corona on the surface of iron oxide nanoparticles (59–65). The particular protein corona that forms around a nanoparticle determines its physicochemical properties, such as its hydrodynamic size and surface charge (66–68), and how it interacts with cells (69,70). For example, protein coronas that contain apolipoproteins ApoB100 and ApoE improve transport of nanoparticles across the blood-brain barrier (71,72), protein coronas that contain immunoglobulins and complement C3b improve nanoparticle uptake by monocytes (73), and protein coronas that contain albumin (74) and CD47 (75) prevent cellular nanoparticle uptake. The effect of the protein corona on cellular nanoparticle uptake and in vivo distribution of diagnostic USPIOs in patients is a largely understudied area.

Iron Oxides Do Not Interact with Gadolinium Chelates

Depending on the administered dose, intravenously injected iron oxide nanoparticles provide long-lasting

vascular enhancement for several days and tissue enhancement for several weeks. This finding has led to concerns regarding potential interactions between iron oxide nanoparticles and gadolinium chelates. Extensive dual–contrast agent imaging studies conducted in more than 1000 patients showed that iron oxide nanoparticles do not interact with or interfere with the pharmacokinetics or imaging characteristics of gadolinium chelates (76–79). Dual–contrast agent MR imaging has been performed after injection of iron oxides and then gadolinium chelates (76,78–80) or vice versa (77). Nevertheless, it will be important to understand tissue MR enhancement patterns after administration of iron oxide nanoparticles (see below). With more than 1 million ferumoxytol administrations for anemia treatment to date, radiologists will likely acquire MR images in ferumoxytol-treated patients. Therefore, we should consider including a question about previous treatments with iron products on MR imaging screening forms.

USPIOs Have Different T1 Enhancement Patterns Compared with Gadolinium Chelates

T1 contrast enhancement due to iron oxide nanoparticles such as ferumoxytol is very different compared with that due to gadolinium chelates in terms of timing, duration, bio-distribution, and elimination from the body (Figs 2, 3). The T1 shortening process requires close interaction between water molecules and iron oxide nanoparticles (81). Small-molecular-weight gadolinium chelates distribute nonspecifically in blood and extracerebral tissues, providing uniform strong T1 enhancement. By contrast, due to their large size, iron oxide nanoparticles do not extravasate in most tissues. This can be harnessed for MR angiography (7,8), long-lasting vascular enhancement in whole-body MR imaging and positron emission tomography/MR imaging tumor staging (82,83), MR imaging of vascular malformations (84), MR imaging of inflammation (31,85), and interestingly, MR detection of early tumor necrosis (10,85). Due to a lower degree and rate of extravasation and a higher drug concentration gradient between vessels and tissues, T1-based steady-state angiography can be performed with iron oxide doses of 1 mg of iron per kilogram or less (24). Higher nanoparticle doses can lead to susceptibility-related signal loss in large vessels, which can impair quantitative MR data analyses and cause artifacts mimicking thrombosis (25).

In the reticuloendothelial system (RES) (ie, liver spleen and bone marrow), ferumoxytol nanoparticles extravasate through discontinuous microvessels and/or sinuses and cause strong T1 enhancement within the first few hours after iron oxide administration (Fig 3). Ferumoxytol tissue T1 enhancement on gradient-echo sequences can be improved by increasing the nanoparticle dose, decreasing the flip angle, and minimizing the echo time (82,86). In most tissues outside of the RES, ferumoxytol does not extravasate and therefore causes substantially lower T1 enhancement of tissues when compared with gadolinium chelates (35). Therefore, ferumoxytol is not well suited for detecting small tumors outside of the RES. Ferumoxytol tumor enhancement during the relatively early perfusion phase, 1–30 minutes after injection, is limited by an average tumor blood volume of about 5%. This is much lower compared with gadolinium chelates, which rapidly distribute to the larger extracellular space (Fig 3). Peak ferumoxytol enhancement in malignant tumors is typically reached at 24–48 hours after intravenous ferumoxytol administration (9). To compensate for the low sensitivity of iron oxide nanoparticles, tumor imaging studies are typically performed with high doses of 5–8 mg of iron per kilogram (11,82).

Iron oxide nanoparticles can provide information for tumor characterization not accessible by gadolinium chelates. By creating a "blood-body barrier" (in analogy to the blood-brain barrier), USPIOs can better characterize differences in the microvascular permeability of benign and malignant breast tumors (23) and other soft-tissue tumors; benign tumors show no or minimal USPIO enhancement, whereas malignant tumors show marked USPIO enhancement (23). In malignant tumors, the degree of ferumoxytol MR imaging enhancement increased with increasing histopathologic grade (23). In the brain, ferumoxytol improved the differentiation between nonenhancing meningiomas and enhancing dural metastases (87), as well as immunotherapy-induced cancer pseudoprogression and true progression (26).

Echo Times Should Be Checked on In-Phase and Opposed-Phase Sequences

Iron oxide nanoparticles shorten T2 and T2* relaxation times of target tissues. This has been classically used for the detection of focal lesions in liver, spleen, lymph nodes, and bone marrow (Fig 4) (12,22,27,82,88,89). T2 shortening effects are due to "outer sphere" effects (proton diffusion-dependent dephasing and signal decay) and/or "inner sphere" effects (chemical exchange between iron-bound and free water protons) (90). T2* effects of iron oxides are due to static dephasing and exceed T2 effects (91). Therefore, T2*-weighted sequences are more sensitive for iron oxide nanoparticle detection. Iron oxide nanoparticle–induced T2* tissue enhancement can be maximized by increasing the applied magnetic field strength by using high iron oxide doses of 3–7 mg per kilogram ferumoxytol (92,93), gradient echo instead of spin echo sequences, and long echo times (91). T2* shortening effects of iron oxide nanoparticles have been used for tissue perfusion studies (92,93), detection of malignant tumors in RES organs (ie, liver, spleen, bone marrow, and lymph nodes) (17–21,79,80) (Figs 4, 5), suppression of false-positive signals of normal spleen and bone marrow on diffusion-weighted images (82), detection of tumor-associated macrophages in cancers (94), artherosclerotic plaque imaging (28–30), imaging of inflammation (31,32), and in vivo cell tracking (91,95–98), among others. Of note, the T1 effect of iron oxides diminishes

Figure 2

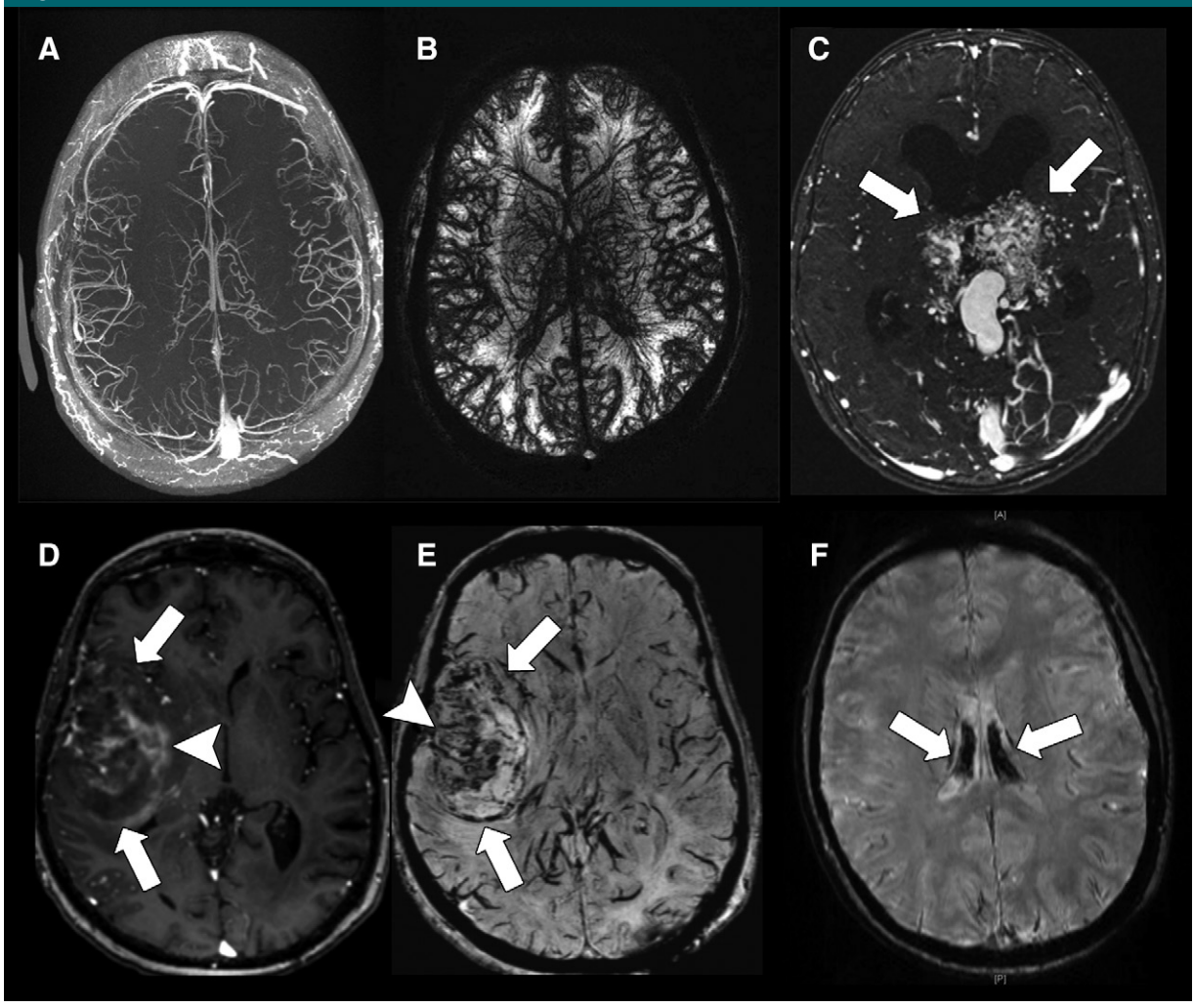

Figure 2: Ferumoxytol-enhanced brain MR imaging. *A, B,* Axial spoiled gradient-recalled-echo (SPGR) images with, *A,* T1 contrast (repetition time msec/echo time msec, 4.5/1.3; flip angle, 15°) and, *B,* T2 contrast (36/15; flip angle, 15°) through the brain of a human volunteer 1–2 hours after intravenous injection of ferumoxytol (dose, 6 mg iron per kilogram of body weight). *C,* Axial T1-weighted SPGR (4.3/1.0; flip angle,15°) image of a bithalamic arteriovenous malformation (arrows) in a 9-year-old girl obtained 1 hour after injection of ferumoxytol at a dose of 3 mg iron per kilogram of body weight. *D,* Axial T1-weighted SPGR (9.5/3.8; flip angle, 13°) and, *E,* susceptibility-weighted SPGR (43.6/4.6; flip angle, 15°) images acquired 2 days after ferumoxytol administration (dose, 5 mg iron per kilogram of body weight) in a 53-year-old female patient show a recurrent glioblastoma in the right temporal lobe (arrows). Different tumor areas show hyperintense T1 enhancement and hypointense T2 enhancement (arrowheads). *F,* Susceptibility-weighted SPGR image (50/5.8; flip angle, 15°) acquired 2 years after an MR imaging scan with ferumoxytol (dose, 5 mg iron per kilogram of body weight) in a 15-year-old female patient with osteosarcoma of the femur and successfully treated recurrence (not shown). The patient had also received multiple blood transfusions after the ferumoxytol scan. The brain MR image, obtained due to chronic headaches, shows hypointense signal of the choroid plexus, consistent with iron deposition (arrows). (Courtesy of Michael Moseley, Thomas Christen, Samantha Holdsworth, Kristen Yeom, and Michael Iv, Stanford University.)

when the nanoparticles are compartmentalized and clustered in cells, while T2 effects decline to a lesser degree and T2* effects remain largely unaffected (91,99). Thus, the combination of T1, T2, and T2* effects allows us to determine the extra- or intracellular nanoparticle location (10,91).

For accurate interpretation of in-phase (IP) and opposed-phase (OP) gradient-echo images after iron oxide nanoparticle administration, it is important to understand the applied echo times: Most commercial 1.5-T imagers use OP-IP gradient-echo sequences, where the first echo time of 2.3 msec generates OP images and the second echo time of 4.6 msec generates IP images (90). With these systems, IP images have longer echo times and show stronger iron oxide enhancement (lower signal) compared with OP images. Therefore, on these OP-IP images, liver and adrenal gland fat show a lower signal on

Figure 3

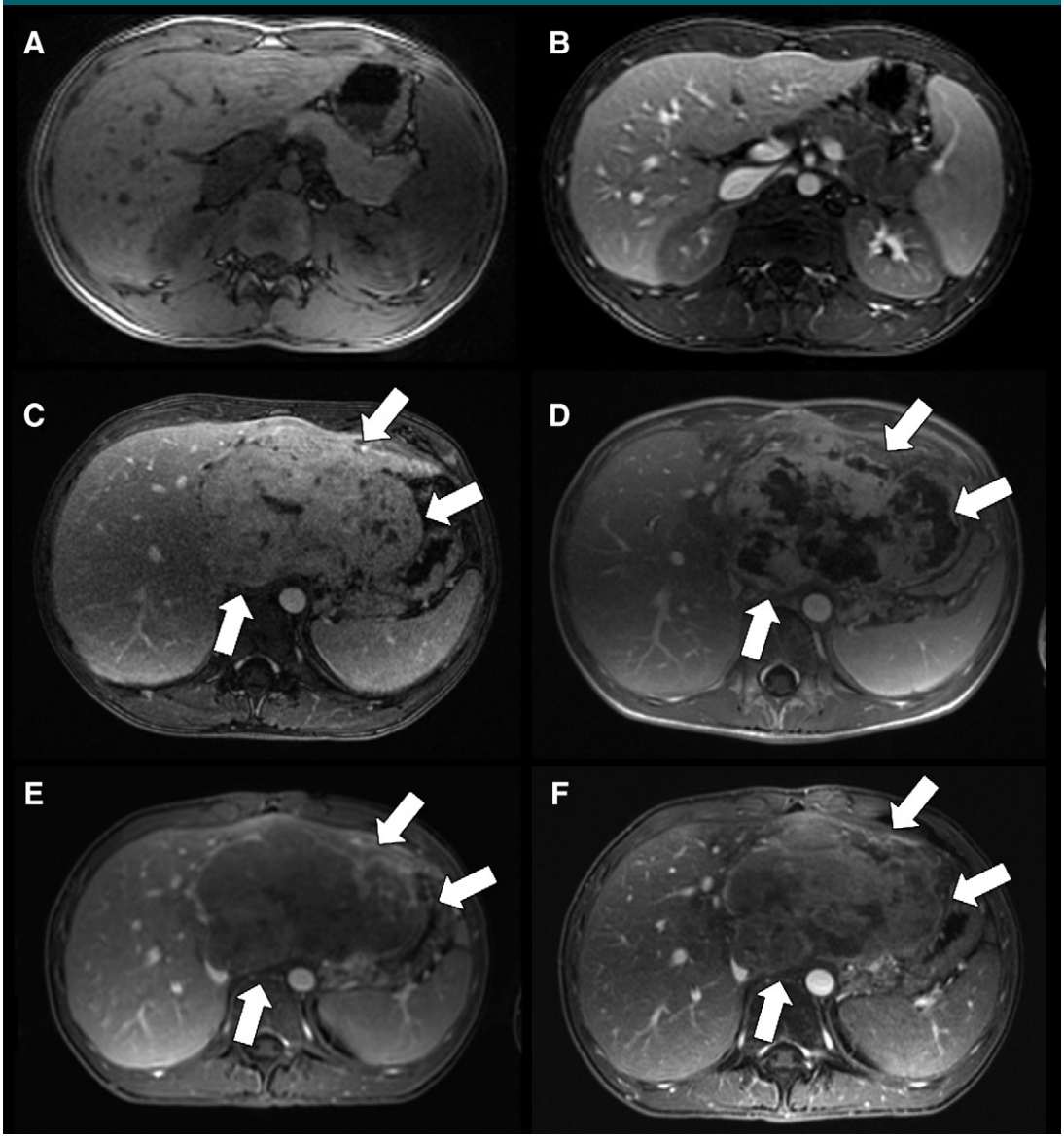

Figure 3: Ferumoxytol-enhanced T1-weighted MR imaging of the abdomen and comparison with gadolinium chelates. *A, B,* Axial T1-weighted fast spoiled gradient-echo (3.3/1.2; flip angle, 15°) sequences through the upper abdomen of a 15-year-old boy before (*A,* nonfat-saturated sequence) and after (*B,* fat-saturated sequence) intravenous infusion of ferumoxytol at a dose of 5 mg iron per kilogram of body weight. Postcontrast images show T1 enhancement of liver, spleen, and kidneys, as well as marked enhancement and improved delineation of abdominal vessels. *C,* Axial T1-weighted liver acquisition with volume acquisition (LAVA) (3.3/1.2; flip angle, 15°) image of a hepatocellular carcinoma (arrows) in a 15-year-old boy after intravenous injection of gadolinium chelate shows marked positive contrast enhancement of both liver and tumor. *D,* Follow-up image after chemoembolization shows marked central necrosis (arrows). *E,* Corresponding MR image after intravenous infusion of ferumoxytol (obtained 1 day after, *C*) shows less tumor enhancement (arrows) and improved vessel delineation around the lesion. *F,* MR image after chemoembolization and intravenous infusion of ferumoxytol shows smaller areas of nonenhancing necrosis (arrows) compared with, *D,* and some tumor areas with increased iron enhancement compared with, *E,* presumably representing early tumor necrosis with increased nanoparticle leak and retention.

OP than IP images (dark-bright signal), and iron oxide nanoparticles show the opposite effect (bright-dark signal).

Conversely, some 3-T imagers use IP-OP gradient-echo sequences, where the first echo time of 2.3 msec generates IP images and the second echo time of 5.8 msec generates OP images (90). With this setup, the OP images have

Figure 4

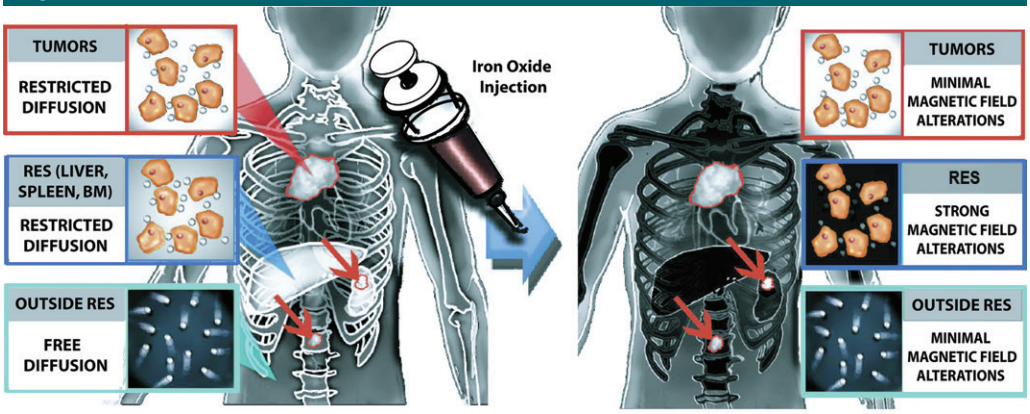

Figure 4: Schematics depict the value of iron oxide nanoparticles for tumor detection on diffusion-weighted MR images. **(a)** Before iron oxide injection, the intrinsic restricted diffusion in spleen and marrow can mask tumor deposits in these organs. **(b)** After iron oxide nanoparticle injection, normal tissues of the RES show negative (dark) T2 enhancement, while focal neoplastic lesions show no or substantiaally less enhancement, leading to improved tumor-to-background contrast.

Figure 5

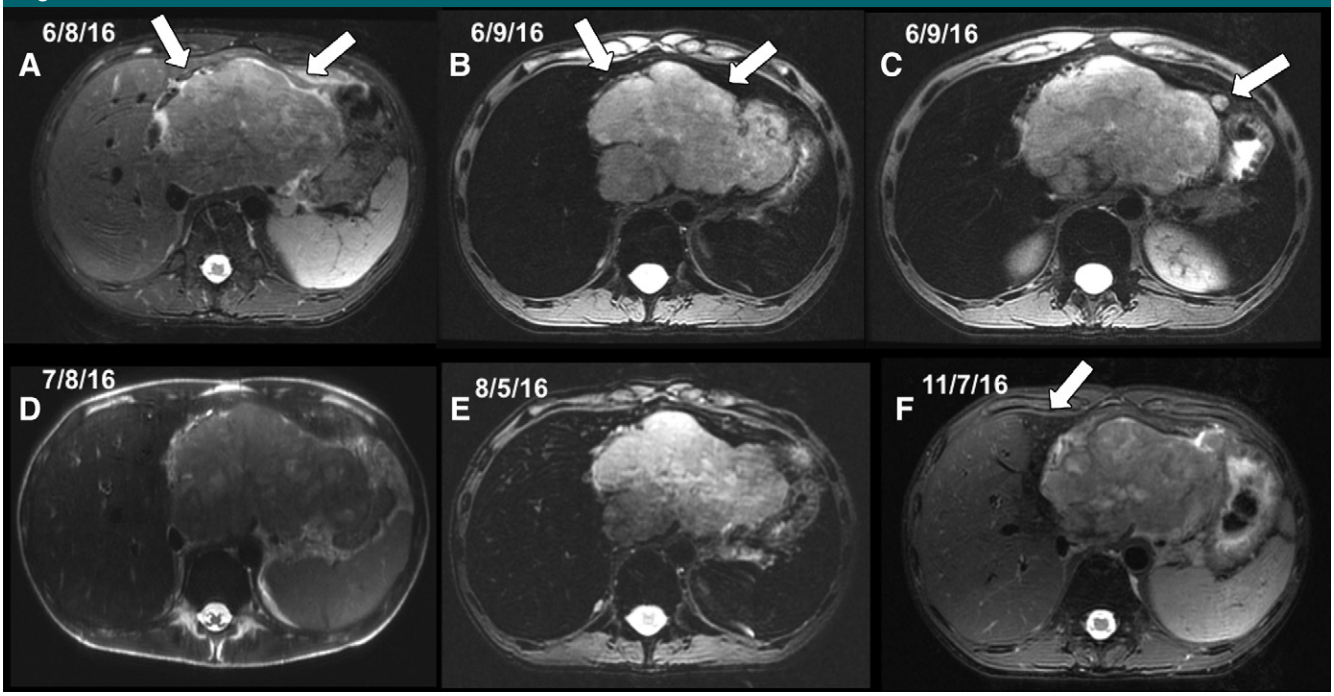

Figure 5: Ferumoxytol-enhanced T2-weighted MR images in a 15-year-old boy with hepatocellular carcinoma before and at different time points after intravenous infusion of ferumoxytol (same patient as in Fig 3). *A,* Axial T2-weighted fast spin-echo (FSE) image (12 000/81) before contrast media administration. *B, C,* T2-weighted FSE (4000/65) images14 hours after intravenous infusion of ferumoxytol at a dose of 5 mg iron per kilogram show marked negative (dark) enhancement of normal liver parenchyma with improved delineation of nonenhancing tumor (arrows, *B*) and a satellite lesion (arrow, *C*). *D,* Follow-up single-shot T2-weighted FSE image (1900/118) 4 weeks later shows some iron metabolization in liver and spleen. *E,* T2-weighted FSE image (4000/65) 22 hours after a second ferumoxytol injection shows similar enhancement to that in *B. F,* Axial T2-weighted FSE image (12 000/81) obtained 8 weeks later shows marked clearance of iron from the right liver lobe and spleen, while the peritumoral left liver lobe shows iron retention (arrow), possibly due to recent chemoembolization. Remaining signal loss is also noted in the bone marrow. Further follow-up studies showed complete clearance of iron from the liver and spleen (not shown).

longer echo times and show stronger iron oxide enhancement. Therefore, on IP-OP images, liver fat and iron oxide nanoparticles show the same effect: a lower signal on OP images than on IP images (bright-dark signal).

Considering the above protocols, the detection of most focal liver lesions would be better on the IP images from OP-IP sequences and OP images from IP-OP sequences, due to better lesion-to-liver contrast on the sequence with the longer echo time.

Iron oxide nanoparticles are slowly degraded by macrophages in the RES (Fig 5). The nanoparticle coating is cleaved by lysosomal enzymes and the iron core is incorporated into the body's iron stores, where it is slowly metabolized over 6–12 weeks (100). Excessive doses of ferumoxytol can lead to long-lasting signal effects on MR images (101) and can potentially cause hemosiderosis (100), although no cases of ferumoxytol-induced hemosiderosis have been described in patients to date. Doses for imaging purposes (1–5 mg of iron per kilogram of body weight) are smaller than doses for anemia treatment (initial 510 mg intravenous injection followed by a second 510 mg injection 3–8 days later) (100). The impact of USPIO biodegradation on T2 and T2* signal is a largely understudied area.

Iron Oxide Nanoparticles Are Retained in Organs Outside of the RES

Outside of the RES, iron oxide nanoparticles are taken up by adrenal glands (34,101), alveolar macrophages in the lungs (102), peritoneal macrophages (58), and synovial membrane macrophages in joints (32,103).

The normal adrenal gland demonstrates marked negative (dark) enhancement on T2-weighted MR images at 1 and 24 hours after ferumoxytol administration (34). By contrast, retroperitoneal tumors show little or no ferumoxytol enhancement (82). This difference in ferumoxytol enhancement between benign adrenal tissue and malignant adrenal masses might prove useful in the differential diagnosis of adrenal lesions. In patients with hemosiderosis and hemochromatosis, iron deposition in the adrenal gland can rarely lead to hypoaldosteronism (104–106). The related effects of iron oxide nanoparticles have not been described.

USPIOs do not cross the blood-brain barrier in healthy subjects. However, brain scans of patients after multiple blood or iron transfusions can show persistent hypointense enhancement in the choroid plexus for days to weeks (107,108) (Fig 1). It is unknown whether ferumoxytol can penetrate through the choroid plexus into the cerebrospinal fluid. In animal models, intravenously administered iron was retained in choroid plexus epithelial cells and in neuroglial cells (107,108). In vitro studies have shown that iron oxide nanoparticle–exposed neuronal stem cells have a near immediate ability to adapt to local changes in iron content by downregulation of transferrin receptor 1 (Tfrc) and heme oxygenase 1 (Hmox1) expression and upregulation of genes involved in lysosomal function (Sulf1) and detoxification (Clu, Cp, Gstm2, Mgst1) (109). Interestingly, this study found no change in gene expression related to apoptosis pathways (109); others have suggested that iron oxides can induce ferroptosis in cancer cells through a caspase-independent cell death pathway (110). Further studies are needed to understand whether cumulative USPIO doses lead to iron deposition in the brain and whether USPIO can cause ferroptosis in patients.

Iron Oxide Nanoparticles Do Not Localize to Macrophages in Lymph Nodes

USPIOs have been used extensively for the detection of lymph node metastases (11,12,15). Previous studies showed that ferumoxtran-10 and ferumoxytol nanoparticles are retained in normal lymph nodes, causing a long-lasting T2 and T2* signal effect on T2- and T2*-weighted MR images 24–48 hours after intravenous injection of USPIOs. Conversely, metastases in lymph nodes did not take up iron oxides and, therefore, could be detected as relative hyperintense lesions. It was suggested that, in accordance with the concept of imaging metastasis in the liver with iron oxides, the T2 effect in normal lymph nodes is due to macrophage phagocytosis. However, despite more than 100 scientific articles on this subject, no study has yet localized iron oxide nanoparticles to specific cellular components in normal lymph nodes. Two studies correlated iron oxide enhancement of reactive and inflamed lymph nodes with histopathologic findings: Xue et al evaluated inflammatory lymph nodes in rabbits after injection of Freund adjuvant (111). The highly inflamed lymph nodes showed retention of iron oxides in macrophages. Koh et al evaluated reactive nodes in patients with colorectal cancer. The authors found decreased T2 signal of reactive nodes on MR images and scattered iron-containing macrophages on corresponding histopathologic specimens (112). Neither of these studies evaluated the localization of iron oxide nanoparticles in the cellular components of normal lymph nodes, which typically contain few macrophages. Since normal lymph nodes contain mostly T cells and only few macrophages, it is unclear which cell type in a healthy lymph node retains SPIO nanoparticles (Fig 6). Other immune cell types capable of phagocytosis, such as dendritic cells, could take up iron oxide nanoparticles and contribute to the observed T2-signal enhancement. This is important because it might enable us to differentiate lymph node pathologies with different immune cell compositions based on their differential iron uptake. Future studies are needed to elucidate if and when iron oxide nanoparticles localize to the intravascular space, the extravascular-interstitial space, or cellular components in healthy lymph nodes. Interestingly, the USPIO uptake in lymph nodes can be substantially enhanced by preadministration or coadministration of nonsteroidal anti-inflammatory drugs (42).

Summary

Since USPIOs are not associated with a risk of nephrogenic sclerosis, they can serve as a safer contrast agents compared with gadolinium chelates

Figure 6

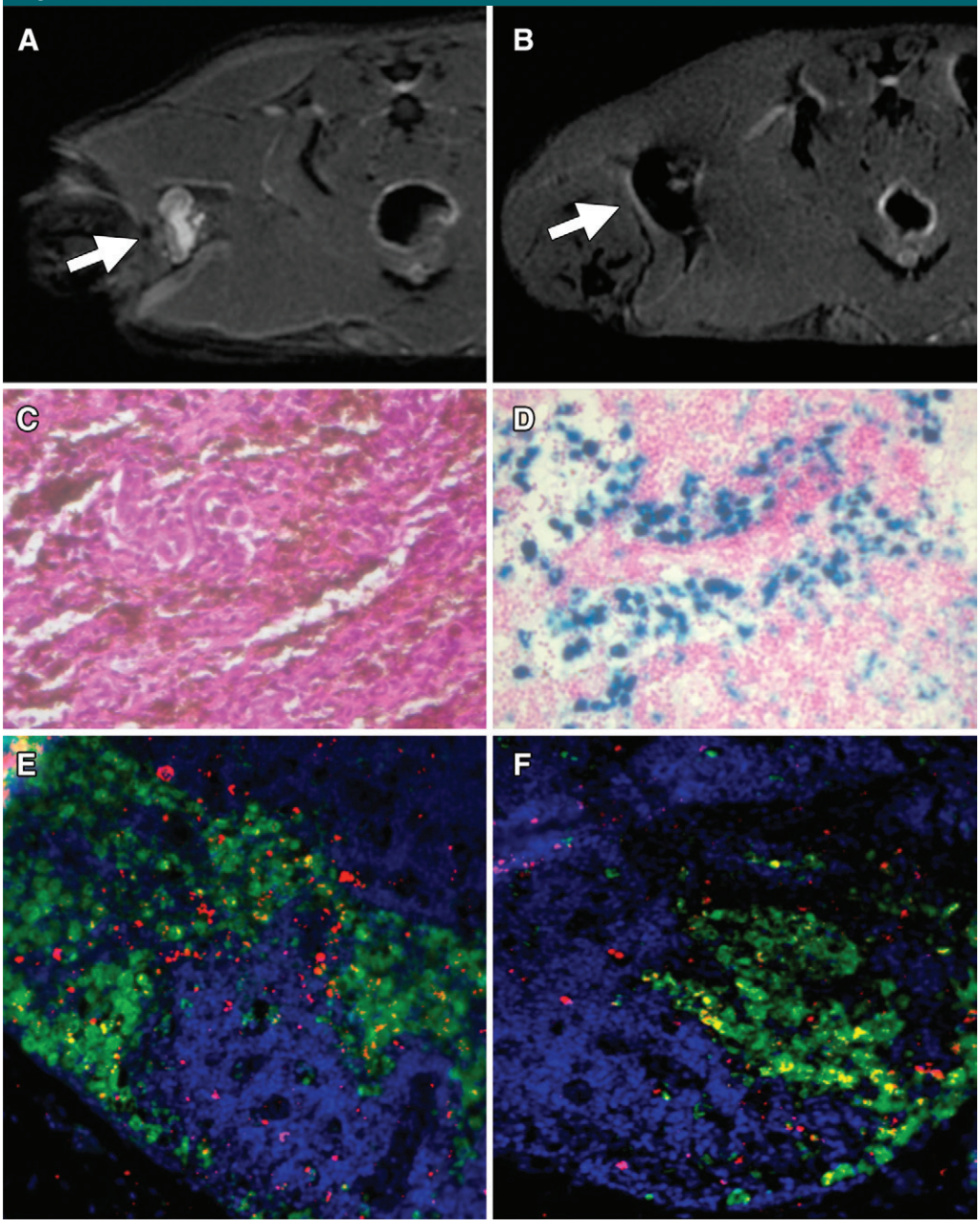

Figure 6: Ferumoxytol-enhanced MR imaging of a normal lymph node with histopathologic correlation. *A,* Axial T2-weighted fast spin-echo (5700/25) image through the lower abdomen of a Sprague-Dawley rat shows normal lymph node in the right inguinal region (arrow). *B,* At 24 hours after intravenous injection of fluorescein isothiocyanate (FITC)-conjugated ferumoxytol at a dose of 30 mg iron per kilogram, the lymph node shows marked signal loss (arrow). *C,* Corresponding hematoxylin-eosin histopathologic slice shows normal lymph node architecture (magnification, ×40). *D,* Prussian blue staining shows iron containing cells (magnification, ×40). *E, F,* Confocal microscopy of the same lymph node shows numerous cells with intracellular FITC ferumoxytol (green) and only few macrophages (red, stained with rhodamin-labeled anti-CD68 mAb; blue = DAPI [49,6-diamidino-2-phenylindole]; magnification, ×40). Not all macrophages contain FITC-ferumoxytol and numerous cells that do contain FITC-ferumoxytol are apparently not macrophages.

for several indications, including MR angiography, tissue perfusion studies, and atherosclerotic plaque and tumor imaging. USPIOs are especially beneficial for patients with renal insufficiency or patients with uncertain creatinine laboratory values. Two USPIOs are currently being used for clinical applications: the FDA-approved iron supplement ferumoxytol and ferumoxtran-10, which is undergoing renewed clinical trials in Europe. Safety considerations for these agents include slow intravenous infusion over at least 15 minutes to avoid hypotensive reactions, possible complication of skin discolorations, and preparedness for rare, but possible severe anaphylactic reactions. Both ferumoxytol and ferumoxtran-10 provide long-lasting blood pool enhancement, which can be used for any MR imaging examination that requires detailed and/or long-lasting vessel delineation such as MR angiographies, tissue perfusion studies, and whole-body tumor staging with MR and positron emission tomography/MR imaging. USPIOs are slowly phagocytosed by macrophages in the RES, making them ideal for MR imaging detection of tumors in the liver, spleen, lymph nodes, and bone marrow. Similarly, USPIOs are slowly phagocytosed by tumor-associated macrophages in the tumor microenvironment; this could be leveraged to grade tumor-associated inflammation and monitor the efficacy of new cancer immunotherapies. Finally, new developments in USPIOs may spur new personalized diagnostic tests and theranostic (combined diagnostic and therapeutic) procedures.

Acknowledgments: I thank Julie Gosse, PhD, for copy editing this article and Fanny Chapelin, MS, Thomas Christen, PhD, Samantha Holdsworth, PhD, Michael Iv, MD, Michael Moseley, PhD, Anne Muehe, MD, Ashok Theruvath, MD, and Kristen Yeom, MD, from the ferumoxytol-imaging team at Stanford University for valuable discussions and for contributing imaging examples to this article.

Disclosures of Conflicts of Interest: H.E.D.L. disclosed no relevant relationships.

References

1. Lauterbur PC, Dias MHM, Rudin AM. Augmentation of tissue water proton spin-lattice relaxation rates by in vivo addition of paramagnetic ions. In: Dutton P, ed. Electrons to tissues. London, England: Academic Press, 1978; 752–759.
2. Weinmann HJ, Laniado M, Mützel W. Pharmacokinetics of GdDTPA/dimeglumine after intravenous injection into healthy volunteers. Physiol Chem Phys Med NMR 1984;16(2):167–172.
3. Laniado M, Weinmann HJ, Schörner W, Felix R, Speck U. First use of GdDTPA/dimeglumine in man. Physiol Chem Phys Med NMR 1984;16(2):157–165.
4. Weinmann HJ, Brasch RC, Press WR, Wesbey GE. Characteristics of gadolinium-DTPA complex: a potential NMR contrast agent. AJR Am J Roentgenol 1984;142(3):619–624.
5. Toth GB, Varallyay CG, Bashir MR, et al. Current and potential imaging applications of ferumoxytol for magnetic resonance imaging. Kidney Int 2017 Apr 14. [Epub ahead of print]
6. Landry R, Jacobs PM, Davis R, Shenouda M, Bolton WK. Pharmacokinetic study of ferumoxytol: a new iron replacement therapy in normal subjects and hemodialysis patients. Am J Nephrol 2005;25(4):400–410.
7. Li W, Tutton S, Vu AT, et al. First-pass contrast-enhanced magnetic resonance angiography in humans using ferumoxytol, a novel ultrasmall superparamagnetic iron oxide (USPIO)-based blood pool agent. J Magn Reson Imaging 2005;21(1):46–52.
8. Li W, Salanitri J, Tutton S, et al. Lower extremity deep venous thrombosis: evaluation with ferumoxytol-enhanced MR imaging and dual-contrast mechanism--preliminary experience. Radiology 2007;242(3):873–881.
9. Neuwelt EA, Várallyay CG, Manninger S, et al. The potential of ferumoxytol nanoparticle magnetic resonance imaging, perfusion, and angiography in central nervous system malignancy: a pilot study. Neurosurgery 2007;60(4):601–611; discussion 611–612.
10. Aghighi M, Golovko D, Ansari C, et al. Imaging tumor necrosis with ferumoxytol. PLoS One 2015;10(11):e0142665.
11. Turkbey B, Agarwal HK, Shih J, et al. A phase I dosing study of ferumoxytol for MR lymphography at 3 T in patients with prostate cancer. AJR Am J Roentgenol 2015;205(1):64–69.
12. Harisinghani MG, Barentsz J, Hahn PF, et al. Noninvasive detection of clinically occult lymph-node metastases in prostate cancer. N Engl J Med 2003;348(25):2491–2499.
13. Heesakkers RA, Hövels AM, Jager GJ, et al. MRI with a lymph-node-specific contrast agent as an alternative to CT scan and lymph-node dissection in patients with prostate cancer: a prospective multicohort study. Lancet Oncol 2008;9(9):850–856.
14. Smits LP, Coolen BF, Panno MD, et al. Noninvasive differentiation between hepatic steatosis and steatohepatitis with MR imaging enhanced with USPIOs in patients with nonalcoholic fatty liver disease: a proof-of-concept study. Radiology 2016;278(3):782–791.
15. Triantafyllou M, Studer UE, Birkhäuser FD, et al. Ultrasmall superparamagnetic particles of iron oxide allow for the detection of metastases in normal sized pelvic lymph nodes of patients with bladder and/or prostate cancer. Eur J Cancer 2013;49(3):616–624.
16. Stark DD, Weissleder R, Elizondo G, et al. Superparamagnetic iron oxide: clinical application as a contrast agent for MR imaging of the liver. Radiology 1988;168(2):297–301.
17. Jung CW, Jacobs P. Physical and chemical properties of superparamagnetic iron oxide MR contrast agents: ferumoxides, ferumoxtran, ferumoxsil. Magn Reson Imaging 1995;13(5):661–674.
18. Reimer P, Rummeny EJ, Daldrup HE, et al. Clinical results with Resovist: a phase 2 clinical trial. Radiology 1995;195(2):489–496.
19. Ros PR, Freeny PC, Harms SE, et al. Hepatic MR imaging with ferumoxides: a multicenter clinical trial of the safety and efficacy in the detection of focal hepatic lesions. Radiology 1995;196(2):481–488.
20. Vogl TJ, Hammerstingl R, Schwarz W, et al. Magnetic resonance imaging of focal liver lesions. Comparison of the superparamagnetic iron oxide resovist versus gadolinium-DTPA in the same patient. Invest Radiol 1996;31(11):696–708.
21. Kopp AF, Laniado M, Dammann F, et al. MR imaging of the liver with Resovist: safety, efficacy, and pharmacodynamic properties. Radiology 1997;204(3):749–756.
22. Harisinghani MG, Saini S, Weissleder R, et al. MR lymphangiography using ultrasmall superparamagnetic iron oxide in patients with primary abdominal and pelvic malignancies: radiographic-pathologic correlation. AJR Am J Roentgenol 1999;172(5):1347–1351.
23. Daldrup-Link HE, Rydland J, Helbich TH, et al. Quantification of breast tumor microvascular permeability with feruglose-enhanced MR imaging: initial phase II multicenter trial. Radiology 2003;229(3):885–892.
24. Ahlström KH, Johansson LO, Rodenburg JB, Ragnarsson AS, Akeson P, Börseth A. Pulmonary MR angiography with ultrasmall superparamagnetic iron oxide particles as

a blood pool agent and a navigator echo for respiratory gating: pilot study. Radiology 1999;211(3):865–869.

25. Fananapazir G, Marin D, Suhocki PV, Kim CY, Bashir MR. Vascular artifact mimicking thrombosis on MR imaging using ferumoxytol as a contrast agent in abdominal vascular assessment. J Vasc Interv Radiol 2014;25(6):969–976.
26. Gahramanov S, Raslan AM, Muldoon LL, et al. Potential for differentiation of pseudoprogression from true tumor progression with dynamic susceptibility-weighted contrast-enhanced magnetic resonance imaging using ferumoxytol vs. gadoteridol: a pilot study. Int J Radiat Oncol Biol Phys 2011;79(2):514–523.
27. Daldrup-Link HE, Rummeny EJ, Ihssen B, Kienast J, Link TM. Iron-oxide-enhanced MR imaging of bone marrow in patients with non-Hodgkin's lymphoma: differentiation between tumor infiltration and hypercellular bone marrow. Eur Radiol 2002;12(6):1557–1566.
28. Herborn CU, Vogt FM, Lauenstein TC, et al. Magnetic resonance imaging of experimental atherosclerotic plaque: comparison of two ultrasmall superparamagnetic particles of iron oxide. J Magn Reson Imaging 2006;24(2):388–393.
29. Schmitz SA, Taupitz M, Wagner S, Wolf KJ, Beyersdorff D, Hamm B. Magnetic resonance imaging of atherosclerotic plaques using superparamagnetic iron oxide particles. J Magn Reson Imaging 2001;14(4):355–361.
30. Yancy AD, Olzinski AR, Hu TC, et al. Differential uptake of ferumoxtran-10 and ferumoxytol, ultrasmall superparamagnetic iron oxide contrast agents in rabbit: critical determinants of atherosclerotic plaque labeling. J Magn Reson Imaging 2005;21(4):432–442.
31. Gaglia JL, Harisinghani M, Aganj I, et al. Noninvasive mapping of pancreatic inflammation in recent-onset type-1 diabetes patients. Proc Natl Acad Sci U S A 2015;112(7):2139–2144.
32. Simon GH, von Vopelius-Feldt J, Fu Y, et al. Ultrasmall supraparamagnetic iron oxide-enhanced magnetic resonance imaging of antigen-induced arthritis: a comparative study between SHU 555 C, ferumoxtran-10, and ferumoxytol. Invest Radiol 2006;41(1):45–51.
33. Vellinga MM, Vrenken H, Hulst HE, et al. Use of ultrasmall superparamagnetic particles of iron oxide (USPIO)-enhanced MRI to demonstrate diffuse inflammation in the normal-appearing white matter (NAWM) of multiple sclerosis (MS) patients: an exploratory study. J Magn Reson Imaging 2009;29(4):774–779.
34. Gunn AJ, Seethamraju RT, Hedgire S, Elmi A, Daniels GH, Harisinghani MG. Imaging behavior of the normal adrenal on ferumoxytol-enhanced MRI: preliminary findings. AJR Am J Roentgenol 2013;201(1):117–121.
35. Daldrup-Link HE, Kaiser A, Helbich T, et al. Macromolecular contrast medium (feruglose) versus small molecular contrast medium (gadopentetate) enhanced magnetic resonance imaging: differentiation of benign and malignant breast lesions. Acad Radiol 2003;10(11):1237–1246.
36. Bailie GR. Comparison of rates of reported adverse events associated with i.v. iron products in the United States. Am J Health Syst Pharm 2012;69(4):310–320.
37. Lu M, Cohen MH, Rieves D, Pazdur R. FDA report: Ferumoxytol for intravenous iron therapy in adult patients with chronic kidney disease. Am J Hematol 2010;85(5):315–319.
38. Finn JP, Nguyen KL, Han F, et al. Cardiovascular MRI with ferumoxytol. Clin Radiol 2016;71(8):796–806.
39. Schiller B, Bhat P, Sharma A. Safety and effectiveness of ferumoxytol in hemodialysis patients at 3 dialysis chains in the United States over a 12-month period. Clin Ther 2014;36(1):70–83.
40. U.S. Food and Drug Administration. FDA Drug Safety Communication: FDA strengthens warnings and changes prescribing instructions to decrease the risk of serious allergic reactions with anemia drug Feraheme (ferumoxytol). http://www.fda.gov/downloads/Drugs/DrugSafety/UCM440336.pdf2015. Accessed January 3, 2017.
41. Rajan TV. The Gell-Coombs classification of hypersensitivity reactions: a re-interpretation. Trends Immunol 2003;24(7):376–379.
42. Kresse M, Pfefferer D, Lawaczek R, Wagner S, Taupitz S, Miyazawa T, Weniger. Include NSAIDs, platelet aggregation inhibitors to improve vascular, lymph node and bone marrow representation of pharmaceutical preparations containing particles, vesicles or polymers. https://www.google.com.au/patents/DE19721947A1?cl=en&hl=de. Released November 26, 1998. Accessed January 3, 2017.
43. Krause W, Gerlach S, Muschick P. Prevention of the hemodynamic effects of iopromide-carrying liposomes in rats and pigs. Invest Radiol 2000;35(8):493–503.
44. Neiser S, Koskenkorva TS, Schwarz K, Wilhelm M, Burckhardt S. Assessment of dextran antigenicity of intravenous iron preparations with Enzyme-Linked Immunosorbent Assay (ELISA). Int J Mol Sci 2016;17(7):E1185.
45. Jahn MR, Andreasen HB, Fütterer S, et al. A comparative study of the physicochemical properties of iron isomaltoside 1000 (Monofer), a new intravenous iron preparation and its clinical implications. Eur J Pharm Biopharm 2011;78(3):480–491.
46. Rampton D, Folkersen J, Fishbane S, et al. Hypersensitivity reactions to intravenous iron: guidance for risk minimization and management. Haematologica 2014;99(11):1671–1676.
47. Szebeni J. Complement activation-related pseudoallergy: a new class of drug-induced acute immune toxicity. Toxicology 2005;216(2-3):106–121.
48. Szebeni J, Baranyi L, Sávay S, et al. Complement activation-related cardiac anaphylaxis in pigs: role of C5a anaphylatoxin and adenosine in liposome-induced abnormalities in ECG and heart function. Am J Physiol Heart Circ Physiol 2006;290(3):H1050–H1058.
49. Hempel JC, Poppelaars F, Gaya da Costa M, et al. Distinct in vitro complement activation by various intravenous iron preparations. Am J Nephrol 2017;45(1):49–59.
50. Van Wyck DB. Labile iron: manifestations and clinical implications. J Am Soc Nephrol 2004;15(Suppl 2):S107–S111.
51. Dager WE, Sanoski CA, Wiggins BS, Tisdale JE. Pharmacotherapy considerations in advanced cardiac life support. Pharmacotherapy 2006;26(12):1703–1729.
52. Lam T, Pouliot P, Avti PK, Lesage F, Kakkar AK. Superparamagnetic iron oxide based nanoprobes for imaging and theranostics. Adv Colloid Interface Sci 2013;199-200:95–113.
53. Chaban VV, Fileti EE. Atomically precise understanding of nanofluids: nanodiamonds and carbon nanotubes in ionic liquids. Phys Chem Chem Phys 2016;18(38):26865–26872.
54. Zanganeh S, Hutter G, Spitler R, et al. Iron oxide nanoparticles inhibit tumour growth by inducing pro-inflammatory macrophage polarization in tumour tissues. Nat Nanotechnol 2016;11(11):986–994.
55. Woodward KN. Origins of injection-site sarcomas in cats: the possible role of chronic inflammation-a review. ISRN Vet Sci 2011;2011:210982.
56. Weinbren K, Salm R, Greenberg G. Intramuscular injections of iron compounds and oncogenesis in man. BMJ 1978;1(6114):683–685.

57. Sindrilaru A, Peters T, Wieschalka S, et al. An unrestrained proinflammatory M1 macrophage population induced by iron impairs wound healing in humans and mice. J Clin Invest 2011;121(3):985–997.

58. Breborowicz A, Polubinska A, Breborowicz M, Simon M, Wanic-Kossowska M, Oreopoulos DG. Peritoneal effects of intravenous iron sucrose administration in rats. Transl Res 2007;149(6):304–309.

59. Tenzer S, Docter D, Rosfa S, et al. Nanoparticle size is a critical physicochemical determinant of the human blood plasma corona: a comprehensive quantitative proteomic analysis. ACS Nano 2011;5(9):7155–7167.

60. Tenzer S, Docter D, Kuharev J, et al. Rapid formation of plasma protein corona critically affects nanoparticle pathophysiology. Nat Nanotechnol 2013;8(10):772–781.

61. Lundqvist M, Stigler J, Elia G, Lynch I, Cedervall T, Dawson KA. Nanoparticle size and surface properties determine the protein corona with possible implications for biological impacts. Proc Natl Acad Sci U S A 2008;105(38):14265–14270.

62. Cedervall T, Lynch I, Foy M, et al. Detailed identification of plasma proteins adsorbed on copolymer nanoparticles. Angew Chem Int Ed Engl 2007;46(30):5754–5756.

63. Kah JC, Grabinski C, Untener E, et al. Protein coronas on gold nanorods passivated with amphiphilic ligands affect cytotoxicity and cellular response to penicillin/streptomycin. ACS Nano 2014;8(5):4608–4620.

64. Cifuentes-Rius A, de Puig H, Kah JC, Borros S, Hamad-Schifferli K. Optimizing the properties of the protein corona surrounding nanoparticles for tuning payload release. ACS Nano 2013;7(11):10066–10074.

65. Kah JC, Chen J, Zubieta A, Hamad-Schifferli K. Exploiting the protein corona around gold nanorods for loading and triggered release. ACS Nano 2012;6(8):6730–6740.

66. Yang L, Shang L, Nienhaus GU. Mechanistic aspects of fluorescent gold nanocluster internalization by live HeLa cells. Nanoscale 2013;5(4):1537–1543.

67. Hühn D, Kantner K, Geidel C, et al. Polymer-coated nanoparticles interacting with proteins and cells: focusing on the sign of the net charge. ACS Nano 2013;7(4):3253–3263.

68. Röcker C, Pötzl M, Zhang F, Parak WJ, Nienhaus GU. A quantitative fluorescence study of protein monolayer formation on colloidal nanoparticles. Nat Nanotechnol 2009;4(9):577–580.

69. Fleischer CC, Payne CK. Nanoparticle-cell interactions: molecular structure of the protein corona and cellular outcomes. Acc Chem Res 2014;47(8):2651–2659.

70. Fleischer CC, Payne CK. Secondary structure of corona proteins determines the cell surface receptors used by nanoparticles. J Phys Chem B 2014;118(49):14017–14026.

71. Kim HR, Andrieux K, Gil S, et al. Translocation of poly(ethylene glycol-co-hexadecyl) cyanoacrylate nanoparticles into rat brain endothelial cells: role of apolipoproteins in receptor-mediated endocytosis. Biomacromolecules 2007;8(3):793–799.

72. Kreuter J. Nanoparticulate systems for brain delivery of drugs. Adv Drug Deliv Rev 2001;47(1):65–81.

73. Moghimi SM, Hunter AC. Recognition by macrophages and liver cells of opsonized phospholipid vesicles and phospholipid headgroups. Pharm Res 2001;18(1):1–8.

74. Cedervall T, Lynch I, Lindman S, et al. Understanding the nanoparticle-protein corona using methods to quantify exchange rates and affinities of proteins for nanoparticles. Proc Natl Acad Sci U S A 2007;104(7):2050–2055.

75. Rodriguez PL, Harada T, Christian DA, Pantano DA, Tsai RK, Discher DE. Minimal "Self" peptides that inhibit phagocytic clearance and enhance delivery of nanoparticles. Science 2013;339(6122):971–975.

76. Heilmaier C, Lutz AM, Bolog N, Weishaupt D, Seifert B, Willmann JK. Focal liver lesions: detection and characterization at double-contrast liver MR Imaging with ferucarbotran and gadobutrol versus single-contrast liver MR imaging. Radiology 2009;253(3):724–733.

77. Simon G, Link TM, Wörtler K, et al. Detection of hepatocellular carcinoma: comparison of Gd-DTPA- and ferumoxides-enhanced MR imaging. Eur Radiol 2005;15(5):895–903.

78. Ward J, Guthrie JA, Scott DJ, et al. Hepatocellular carcinoma in the cirrhotic liver: double-contrast MR imaging for diagnosis. Radiology 2000;216(1):154–162.

79. Hanna RF, Kased N, Kwan SW, et al. Double-contrast MRI for accurate staging of hepatocellular carcinoma in patients with cirrhosis. AJR Am J Roentgenol 2008;190(1):47–57.

80. Guiu B, Loffroy R, Ben Salem D, et al. Combined SPIO-gadolinium magnetic resonance imaging in cirrhotic patients: negative predictive value and role in screening for hepatocellular carcinoma. Abdom Imaging 2008;33(5):520–528.

81. Rümenapp C, Gleich B, Haase A. Magnetic nanoparticles in magnetic resonance imaging and diagnostics. Pharm Res 2012;29(5):1165–1179.

82. Klenk C, Gawande R, Uslu L, et al. Ionising radiation-free whole-body MRI versus (18)F-fluorodeoxyglucose PET/CT scans for children and young adults with cancer: a prospective, non-randomised, single-centre study. Lancet Oncol 2014;15(3):275–285.

83. Aghighi M, Pisani LJ, Sun Z, et al. Speeding up PET/MR for cancer staging of children and young adults. Eur Radiol 2016;26(12):4239–4248.

84. Dósa E, Tuladhar S, Muldoon LL, Hamilton BE, Rooney WD, Neuwelt EA. MRI using ferumoxytol improves the visualization of central nervous system vascular malformations. Stroke 2011;42(6):1581–1588.

85. Seyfer P, Pagenstecher A, Mandic R, Klose KJ, Heverhagen JT. Cancer and inflammation: differentiation by USPIO-enhanced MR imaging. J Magn Reson Imaging 2014;39(3):665–672.

86. Simon G, Daldrup-Link H, von Vopelius-Feldt J, et al. MRI of arthritis with the USPIO SH U 555 C: optimization of T1 enhancement [in German]. Rofo 2006;178(2):200–206.

87. Hamilton BE, Woltjer RL, Prola-Netto J, et al. Ferumoxytol-enhanced MRI differentiation of meningioma from dural metastases: a pilot study with immunohistochemical observations. J Neurooncol 2016;129(2):301–309.

88. Weissleder R. Liver MR imaging with iron oxides: toward consensus and clinical practice. Radiology 1994;193(3):593–595.

89. Daldrup HE, Reimer P, Rummeny EJ, et al. New super-paramagnetic iron particles for MRI. Phase II study of malignant liver tumors [in German]. Radiologe 1995;35(8):486–493.

90. Sirlin CB, Reeder SB. Magnetic resonance imaging quantification of liver iron. Magn Reson Imaging Clin N Am 2010;18(3):359–381, ix.

91. Henning TD, Wendland MF, Golovko D, et al. Relaxation effects of ferucarbotran-labeled mesenchymal stem cells at 1.5T and 3T: discrimination of viable from lysed cells. Magn Reson Med 2009;62(2):325–332.

92. Christen T, Ni W, Qiu D, et al. High-resolution cerebral blood volume imaging in humans using the blood pool contrast agent ferumoxytol. Magn Reson Med 2013;70(3):705–710.

93. Varallyay CG, Nesbit E, Fu R, et al. High-resolution steady-state cerebral blood volume maps in patients with central nervous

system neoplasms using ferumoxytol, a superparamagnetic iron oxide nanoparticle. J Cereb Blood Flow Metab 2013;33(5):780–786.

94. Daldrup-Link HE, Golovko D, Ruffell B, et al. MRI of tumor-associated macrophages with clinically applicable iron oxide nanoparticles. Clin Cancer Res 2011;17(17):5695–5704.

95. Khurana A, Chapelin F, Beck G, et al. Iron administration before stem cell harvest enables MR imaging tracking after transplantation. Radiology 2013;269(1):186–197.

96. Townson JL, Ramadan SS, Simedrea C, et al. Three-dimensional imaging and quantification of both solitary cells and metastases in whole mouse liver by magnetic resonance imaging. Cancer Res 2009;69(21):8326–8331.

97. Bulte JW, Douglas T, Witwer B, et al. Magnetodendrimers allow endosomal magnetic labeling and in vivo tracking of stem cells. Nat Biotechnol 2001;19(12):1141–1147.

98. de Vries IJ, Lesterhuis WJ, Barentsz JO, et al. Magnetic resonance tracking of dendritic cells in melanoma patients for monitoring of cellular therapy. Nat Biotechnol 2005;23(11):1407–1413.

99. Simon GH, Bauer J, Saborovski O, et al. T1 and T2 relaxivity of intracellular and extracellular USPIO at 1.5T and 3T clinical MR scanning. Eur Radiol 2006;16(3):738–745.

100. AMAG Pharmaceuticals, Inc. Highlights of Prescribing Information for Feraheme. http://www.accessdata.fda.gov/drugsatfda_docs/label/2009/022180lbl.pdf. Published 2017. Accessed January 3, 2017.

101. Harman A, Chang KJ, Dupuy D, Rintels P. The long-lasting effect of ferumoxytol on abdominal magnetic resonance imaging. J Comput Assist Tomogr 2014;38(4):571–573.

102. Card JW, Zeldin DC, Bonner JC, Nestmann ER. Pulmonary applications and toxicity of engineered nanoparticles. Am J Physiol Lung Cell Mol Physiol 2008;295(3):L400–L411.

103. Simon GH, von Vopelius-Feldt J, Wendland MF, et al. MRI of arthritis: comparison of ultrasmall superparamagnetic iron oxide vs. Gd-DTPA. J Magn Reson Imaging 2006;23(5):720–727.

104. Vantyghem MC, Dobbelaere D, Mention K, Wemeau JL, Saudubray JM, Douillard C. Endocrine manifestations related to inherited metabolic diseases in adults. Orphanet J Rare Dis 2012;7:11.

105. Thomas JP. Aldosterone deficiency in a patient with idiopathic haemochromatosis. Clin Endocrinol (Oxf) 1984;21(3):271–277.

106. Ramírez Montesinos R, Auguet Quintillá MT, Sempere Dura T, García JF, Richart Jurado C. Adrenal hemosiderosis [in Spanish]. Med Clin (Barc) 2007;129(19):760.

107. Morris CM, Keith AB, Edwardson JA, Pullen RG. Uptake and distribution of iron and transferrin in the adult rat brain. J Neurochem 1992;59(1):300–306.

108. Kira R, Ohga S, Takada H, Gondo K, Mihara F, Hara T. MR choroid plexus sign of iron overload. Neurology 2000;55(9):1340.

109. Kedziorek DA, Muja N, Walczak P, et al. Gene expression profiling reveals early cellular responses to intracellular magnetic labeling with superparamagnetic iron oxide nanoparticles. Magn Reson Med 2010;63(4):1031–1043.

110. Kim SE, Zhang L, Ma K, et al. Ultrasmall nanoparticles induce ferroptosis in nutrient-deprived cancer cells and suppress tumour growth. Nat Nanotechnol 2016;11(11):977–985.

111. Xue HD, Lei J, Li Z, et al. Lymph node image with ultrasmall superparamagnetic iron oxide and comparison with pathological result [in Chinese]. Zhongguo Yi Xue Ke Xue Yuan Xue Bao 2009;31(2):139–145.

112. Koh DM, Brown G, Temple L, et al. Rectal cancer: mesorectal lymph nodes at MR imaging with USPIO versus histopathologic findings--initial observations. Radiology 2004;231(1):91–99.

113. Muehe AM, Feng D, von Eyben R, et al. Safety report of ferumoxytol for magnetic resonance imaging in children and young adults. Invest Radiol 2016;51(4):221–227.